Medical Physics Letter

Scaling law for noise variance and spatial resolution in differential phase contrast computed tomography

Guang-Hong Chen,[a] Joseph Zambelli, Ke Li, Nicholas Bevins, and Zhihua Qi
Department of Medical Physics, University of Wisconsin-Madison, Madison, Wisconsin 53705

(Received 13 September 2010; revised 14 December 2010; accepted for publication 14 December 2010; published 7 January 2011)

Purpose: The noise variance versus spatial resolution relationship in differential phase contrast (DPC) projection imaging and computed tomography (CT) are derived and compared to conventional absorption-based x-ray projection imaging and CT.
Methods: The scaling law for DPC-CT is theoretically derived and subsequently validated with phantom results from an experimental Talbot–Lau interferometer system.
Results: For the DPC imaging method, the noise variance in the differential projection images follows the same inverse-square law with spatial resolution as in conventional absorption-based x-ray imaging projections. However, both in theory and experimental results, in DPC-CT the noise variance scales with spatial resolution following an inverse linear relationship with fixed slice thickness.
Conclusions: The scaling law in DPC-CT implies a lesser noise, and therefore dose, penalty for moving to higher spatial resolutions when compared to conventional absorption-based CT in order to maintain the same contrast-to-noise ratio. © *2011 American Association of Physicists in Medicine*. [DOI: 10.1118/1.3533718]

I. INTRODUCTION

Differential phase contrast (DPC) imaging and the extension to computed tomography (CT) have attracted recent interest due to their successful implementation using low brilliance sources.[1–8] Initial experimental results demonstrate that DPC-CT imaging may have the potential to quantitatively measure the composition of a material[7] with superior contrast-to-noise ratio (CNR) when compared to conventional absorption CT imaging.[8,9] In order to address whether the sensitivity of the DPC-CT measurements is sufficient for a specific imaging task, two relationships must be studied: The noise variance dependence on exposure level and the noise variance dependence on spatial resolution. The determination of the first relationship is critical if DPC-CT is to be considered for biomedical applications, where the minimization of radiation dose is paramount. The second relationship, noise variance vs spatial resolution, will determine whether sufficient CNR can be generated at high spatial resolutions and acceptable dose levels. As the spatial resolution is increased to improve fine-object visualization, the noise variance increases, generally following an inverse-power law. The power is different for projection and tomographic imaging in absorption x-ray imaging and has not been fully investigated in the case of DPC and DPC-CT. After determining the above two relationships, the potential advantages of DPC and DPC-CT over conventional x-ray imaging will become clear, allowing for proper selection of applications.

Recently, the first relationship has been addressed for both DPC projection imaging[10] and DPC-CT.[8] It was demonstrated that the noise variance in both DPC and DPC-CT imaging is inversely proportional to radiation dose, which is similar to the relationship in conventional absorption x-ray imaging,[11,12] even though the physical mechanism of image formation is dramatically different.

In this letter, we demonstrate that the noise variance is inversely proportional to the in-plane spatial resolution in DPC-CT. This is in stark contrast with conventional absorption CT, where noise variance is inversely proportional to the third power of in-plane spatial resolution.[13] This behavior indicates that for the same noise variance level, DPC-CT imaging may enable higher spatial resolution than absorption CT. In the following, we will present a theoretical analysis of the relationship between noise variance and spatial resolution. Experimental phantom results are then presented to validate the theoretical analysis.

II. BASIC IMAGING PRINCIPLES OF DPC-CT

In order to study the noise variance-spatial resolution relationship, a Talbot–Lau interferometer DPC and DPC-CT data acquisition setup is used. In this setup, a partially coherent x-ray beam is diffracted by a phase grating with a π-phase shift at the mean beam energy. There will be a self-image formed at the fractional Talbot distance[1,14,15]

$$d = \frac{2m-1}{16} Z_T, \tag{1}$$

where $m=1,2,3,\ldots$ and $Z_T=2p^2/\lambda$ is the Talbot distance, determined by the wavelength λ and the pitch p of the phase grating. In order to record the diffracted beam modulation, a homodyne technique is introduced at the fractional Talbot

distance.[16] An absorption grating with the same period as the diffracted beam modulation pattern ($p_2=p/2$) is used to analyze the beam modulation. After the homodyne analysis, the modulation profile is both low-pass filtered and recorded by the detector elements. At each detector element (u,v), where u is along the transverse direction and v is along the axial direction, it is assumed that the detector count is proportional to the number photons N. N can be approximated by the first two coefficients of the Fourier expansion[1–4,10,17]

$$N(u,v)=N_0+N_1\cos\left[\frac{2\pi}{p_2}x+\phi(u,v)\right], \tag{2}$$

where N_0 and N_1 are given by $N_0=IDhq_0$ and $N_1=IDhq_1$, where I is the measured photon flux, D is the detector width, h is the detector height, and q_n is the nth order Fourier coefficient of the normalized final intensity pattern after the absorption grating. The measured phase shift $\phi(u,v)$ in Eq. (2) is related to the phase change Φ of the x-ray wave induced by the image object by

$$\phi(u,v)=\frac{\lambda d}{p_2}\frac{\partial\Phi}{\partial x}=-\frac{2\pi d}{p_2}\frac{\partial}{\partial x}\int dl\,\delta(x,y,z), \tag{3}$$

where δ is the decrement of the refractive index $n=1-\delta+i\beta$. Therefore, once phase shifts, $\phi(u,v)$ in Eq. (2), are measured from different view angles around the image object, an image of the local distribution of the refractive index decrement can be reconstructed.[3,18,19] In this letter, $\phi(u,v)$ is referred to as the differential projection data and Eq. (3) is referred as the fundamental imaging equation of DPC-CT, connecting a measurable quantity $[\phi(u,v)]$ to a line integral of spatial derivative of $\delta(x,y,z)$.

II.A. Noise model of DPC projection data

In order to measure $\phi(u,v)$, a phase-stepping method[1,17] is used in which the analyzer grating is translated by a fraction of the grating pitch along the x_g axis: $x_g=kp_2/M$ $(k=1,2,\ldots,M)$. The measured number of photons at each phase step is given by

$$N^{(k)}(u,v)=N_0+N_1\cos\left[\frac{2\pi}{M}k+\phi(u,v)\right]. \tag{4}$$

By multiplying both sides of Eq. (4) by $\exp(-i2\pi k/M)$ and summing over k, one obtains

$$e^{i\phi(u,v)}=\frac{2}{MN_1}\sum_{k=1}^{M}N^k(u,v)\exp\left(-i\frac{2\pi k}{M}\right), \tag{5}$$

from which follows

$$\tan[\phi(u,v)]=-\frac{\sum_{k=1}^{M}N^{(k)}\sin(2\pi k/M)}{\sum_{k=1}^{M}N^{(k)}\cos(2\pi k/M)}. \tag{6}$$

Namely, after a Fourier transform of the measured profile over all phase steps, one can obtain the desired differential projection data.

Due to photon number fluctuations, the differential projection data will fluctuate about a mean value $\bar{\phi}$, i.e., $\phi=\bar{\phi}\pm\Delta\phi$. Assuming Poisson statistics in the photon number $N^{(k)}$ and using standard error propagation, one can calculate that the noise variance σ_ϕ^2 of the differential projection data is determined by the noise variance $\sigma_{N^{(k)}}^2=\bar{N}^{(k)}$ of the measurement at each phase step

$$\begin{aligned}\sigma_\phi^2&=\left[\frac{\partial\tan(\phi)}{\partial\phi}\right]^{-2}_{\phi=\bar{\phi}}\sigma^2_{\tan(\phi)}\\&=\cos^4(\bar{\phi})\sum_{k=1}^{M}\left[\frac{\partial\tan(\phi)}{\partial N^{(k)}}\right]^2_{N^{(k)}=\bar{N}^{(k)}}\sigma^2_{N^{(k)}}\\&=\frac{2\bar{N}_0}{M\bar{N}_1^2}=\frac{2}{\epsilon^2}\times\frac{1}{M\bar{N}_0}=\frac{2}{\epsilon^2}\times\frac{1}{M\bar{I}_0Dhq_0},\end{aligned} \tag{7}$$

where

$$\epsilon=\frac{q_1}{q_0}. \tag{8}$$

Here, the parameter ϵ describes the effective efficiency of the interferometer.[20] From Eq. (7), one can see that the noise variance of the differential projection data is inversely proportional to the detected total mean photon number $M\bar{N}_0$ at a given projection view angle. It is also inversely proportional to the square of the efficiency of the interferometer, meaning that higher interferometer efficiency will result in lower noise variance in the differential projection data.

When an image object rotates, the projection data are measured from different directions, resulting in data at different view angles being uncorrelated. As a result, the image noise in the differential projection data has a white-noiselike behavior

$$\overline{\Delta\phi_j\Delta\phi_k}=\sigma_\phi^2\delta_{jk}, \tag{9}$$

where $\delta_{jk}=1$ for $j=k$ and $\delta_{jk}=0$ for $j\neq k$ and $\overline{\Delta\phi_j\Delta\phi_k}$ is the correlation of the projection data with respect to view angle. The indices j,k denote the view angle index in the DPC-CT data acquisition. This property is similar to conventional absorption CT, where the projection data also demonstrates a white noise behavior.[11]

II.B. Spatial resolution dependence of noise variance in DPC-CT

Using the derived noise model for DPC-CT, we can analyze how the noise variance is related to spatial resolution in DPC-CT imaging. DPC-CT images can be directly reconstructed using filtered backprojection with a Hilbert filtering kernel[4,18,19,21]

$$\delta(x,y)=\int_0^\pi d\theta F(\theta,\rho=x\cos\theta+y\sin\theta), \tag{10}$$

where the filtering step F is defined by

$$F(\theta,\rho)=\frac{p_2}{2\pi d}\int_{-\omega_N}^{+\omega_N}d\omega\left[\frac{\mathrm{sgn}(\omega)}{2\pi i}\tilde{\phi}(\omega,\theta)\right]e^{i2\pi\omega\rho}, \tag{11}$$

where $\omega_N=1/(2\Delta x)$ is the bandwidth of Nyquist frequency, determined by the target spatial resolution Δx of the reconstructed images. In Eq. (11), $\tilde{\phi}(\omega,\theta)$ is the Fourier transform of the differential projection data $\phi(u,v)$ at view angle θ. Based on this definition, the noise variance of the reconstructed image at image pixel (x,y) is

$$\sigma_\delta^2(x,y)=\left(\frac{p_2}{4\pi^2 d}\right)^2\int\int d\theta_j d\theta_k\int\int d\omega_j d\omega_k \times \mathrm{sgn}(\omega_j)\mathrm{sgn}(\omega_k)\overline{\Delta\tilde{\phi}(\omega_j,\theta_j)\Delta\tilde{\phi}^*(\omega_k,\theta_k)} \times e^{i2\pi x(\omega_j\cos\theta_j-\omega_k\cos\theta_k)}\times e^{i2\pi y(\omega_j\sin\theta_j-\omega_k\sin\theta_k)}. \tag{12}$$

Using Eq. (9), one can demonstrate that the Fourier transform of the white noise is given by

$$\begin{aligned}\overline{\Delta\tilde{\phi}(\omega_j,\theta_j)\Delta\tilde{\phi}^*(\omega_k,\theta_k)}&=\int\int d\rho_j d\rho_k\overline{\Delta\phi(\rho_j,\theta_j)\Delta\phi^*(\rho_k,\theta_k)}\times e^{-i2\pi(\omega_j\rho_j-\omega_k\rho_k)}\\&=\int\int d\rho_j d\rho_k(\sigma_\phi^2\delta_{ik})e^{-i2\pi(\omega_j\rho_j-\omega_k\rho_k)}\\&=\int\int d\rho_j d\rho_k[\sigma_\phi^2\Delta\theta\Delta\rho\delta(\rho_j-\rho_k)\times\delta(\theta_j-\theta_k)]e^{-i2\pi(\omega_j\rho_j-\omega_k\rho_k)}\\&=\frac{\pi D\sigma_\phi^2}{N_\theta}\delta(\theta_j-\theta_k)\delta(\omega_j-\omega_k),\end{aligned} \tag{13}$$

where D is the detector element width and N_θ is the total number of view angles. Using the above relationship, Eq. (12) can be simplified to

$$\sigma_\delta^2(x,y)=\frac{D\sigma_\phi^2}{16\pi^2 N_\theta}\left(\frac{p_2}{d}\right)^2\int_{-\omega_N}^{+\omega_N}1d\omega=\left(\frac{p_2}{4\pi d}\right)^2\frac{\sigma_\phi^2 D}{N_\theta\Delta x}. \tag{14}$$

After substitution for σ_ϕ^2, as given by Eq. (7), the noise variance-spatial resolution relationship is given

$$\sigma_\delta^2(x,y)=\frac{1}{8}\left(\frac{p_2}{\pi d\epsilon}\right)^2\frac{1}{N_\theta M q_0\bar{I}_0}\frac{1}{h\Delta x}. \tag{15}$$

From Eq. (15), one can see that the noise variance of the DPC-CT image is dependent on several factors. It is inversely proportional to the square of the grating efficiency and also inversely proportional to the total photon flux $N_\theta M\bar{I}_0$ during an image acquisition. Most importantly, Eq. (15) says that for a given system efficiency and design, along with a fixed slice thickness and number of photons measured in a complete acquisition, the noise variance of the DPC-CT image inversely proportional to the in-plane spatial resolution of the reconstruction.

III. EXPERIMENTAL METHODS AND RESULTS

In order to validate the theoretical analysis, we use an experimental Talbot–Lau interferometer system constructed at the University of Wisconsin-Madison. The data acquisition system consists of three x-ray gratings, a rotating-anode x-ray tube (G1592, Varian Medical Systems, California, USA) with a 0.3 mm nominal focal spot connected to a generator (Indico 100, CPI, Ontario, Canada), a CMOS flat panel x-ray detector (Rad-icon, Shad-o-Box 2048, California, USA) with 48 μm primitive detector pitch with 1024 pixels in the v direction and 2048 pixels in the u direction, and a rotating motion stage to enable tomographic acquisitions. The three x-ray gratings were fabricated at the University of Wisconsin-Madison using similar techniques as described in literature.[22] The phase grating has pitch p_1 of 8.0 μm and was designed to introduce the differential π-phase shift with a 50% duty cycle at a mean beam energy of 28 keV. The analyzer grating has a pitch p_2 of 4.5 μm. In this work, eight phase steps were used, sampled over the 4.5 μm period. The noise properties were measured in a water-filled phantom chamber with an outer diameter of 25.5 mm and wall thickness of 1.60 mm.

To acquire a complete data set for CT reconstruction, 360 views of projection data were taken at 1° increments. Each projection had a total exposure time of 40 s, divided over eight phase steps. The tube potential was 40 kVp, with a continuous tube current of 8 mA. Once the intensity modulation was recorded, the data were processed to extract the differential phase and absorption projections.

Prior to reconstruction, the detector pixels were binned along the horizontal directions 1×1, 2×1, 3×1, 4×1, and 5×1 to explore noise variance dependence on spatial resolution. The DPC-CT images were reconstructed using the FBP algorithm outlined in Eq. (10) and (11), while the absorption CT images were reconstructed using a standard FBP algorithm.[13] Two identical scans were performed and the reconstructions were subtracted to obtain a noise-only image. The subtracted image was divided by $\sqrt{2}$ to account for the additive noise incurred from the subtraction of two independent volumes. The variance was measured within a circular ROI of the same region of each subtraction image. The ROI sizes were 180 239, 44 950, 19 870, 11 168, and 7164 pixels for 1×1, 2×1, 3×1, 4×1, and 5×1 binning, respectively. Due to a geometrical magnification factor of 1.2, the reconstructed voxel dimensions range from $40\times40\times40$ to $200\times200\times40$ μm^3. The in-plane resolution is represented by the 10% MTF level of the reconstructed images. The MTF was measured using an absorption reconstruction (at each binning level) of a 15 μm tungsten wire.[23] The spatial frequency f at the 10% MTF level, expressed in units of lp/mm, was converted to a spatial resolution Δx through the relation $\Delta x=1/2f$.

Figure 1 presents experimental data to demonstrate the relative variance dependence on spatial resolution. In order to measure the variance, the standard deviation was measured in the water background and then squared. The logarithm of the measured data was calculated and fit to a linear

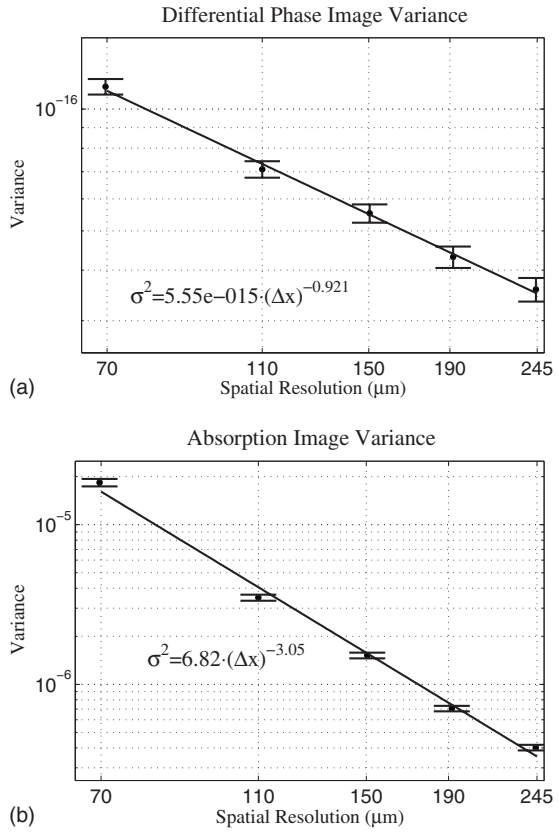

FIG. 1. Log-log plots of relative noise variance against spatial resolution. (a) shows the DPC-CT results, where the fitted curve is of the form $\sigma^2 \propto \Delta x^{-0.921}$, with $R^2=0.998$. (b) shows the absorption CT results, where the fitted curve is of the form $\sigma^2 \propto \Delta x^{-3.05}$, with $R^2=0.994$. Note that the use of a log-log plot results in a linear display of the data, where the exponent of the fit becomes the slope of the curve.

function against the logarithm of spatial resolution using a least-squares method. The slope of the resulting fit is equivalent to the exponential dependence of the measured data on spatial resolution. As shown in Fig. 1(a), for DPC-CT, the noise variance increases with the increase of spatial resolution as $\sigma^2_{\mathrm{PCCT}} \propto (\Delta x)^{-0.921}$, indicating that the noise variance is inversely proportional to the spatial resolution, as derived in Eq. (14). In contrast, for absorption CT [Fig. 1(b)], the noise variance changes with spatial resolution as $\sigma^2_{\mathrm{ACT}} \propto (\Delta x)^{-3.05}$. The error bars in both plots are from repeating the noise measurement for 100 slices within the reconstructed image volume.

IV. DISCUSSION

In the theoretical derivation, we demonstrated that the noise variance in DPC imaging is inversely proportional to photon number. Because the number of photons is proportional to the area of the detector elements at a fixed photon flux, the noise variance of the DPC projection data is proportional to the inverse of detector area. It is well known that the same property is found in absorption projection imaging.[11] The objective of a tomographic reconstruction is to restore the depth information which is lost in projection data due to the line integral along the depth direction. This process is similar for conventional absorption and DPC imaging. In the case of tomographic reconstruction for absorption imaging, the calculation of μ introduces an additional $1/\Delta x$ dependence in the noise of the measurement. This leads to an additional dependence of $1/\Delta x^2$ in the noise variance of μ. The net dependence is therefore $1/\Delta x^4$ for isotropic voxels or $1/\Delta x^3$ for fixed slice thickness, as demonstrated in this paper.

In the case of DPC-CT, the reconstruction of δ does not introduce a net spatial resolution dependence in the noise of the measurement, as shown in Eq. (14). This leads to a final spatial resolution dependence in the noise variance of δ of $1/\Delta x^2$ for isotropic voxels or $1/\Delta x$ for fixed slice thickness, as demonstrated in this paper.

Because the main conclusion of the paper is determined by the differential nature of the measurement of δ, the same conclusion of the relationship between noise and spatial resolution can be drawn for diffraction enhanced CT imaging[21] and neutron imaging,[24] as each also measures refraction angle data. The data are similarly related to the derivative of a line integral as in Eq. (3).

One potential limitation of this study is the extension of the results to spatial resolutions on the order of the pitch of the gratings. Currently, the spatial resolution is limited due to the large focal spot size (0.3 mm) and detector pitch (48 μm). When the focal spot size and the detector pitch are scaled down to the size of the grating pitches, the pitches of the gratings may become the limiting factors to the spatial resolution. In this regime, it is unclear whether the noise variance versus spatial resolution relationship derived in this work remains valid.

V. CONCLUSION

In conclusion, we have theoretically predicted and experimentally validated a scaling relationship between noise variance and spatial resolution. This scaling law dictates that the noise penalty is drastically reduced for high spatial resolution DPC-CT imaging when compared to absorption CT, while at the same time showing that absorption CT benefits more from degraded spatial resolution. Because there is a smaller noise penalty at high spatial resolution, a smaller radiation dose is needed to maintain sufficient CNR for visualization. This is an advantage over conventional absorption CT, where the dose penalty often hinders the application of CT in high spatial resolution imaging.

ACKNOWLEDGMENTS

This work was partially funded by NIH Training Grant No. 5T32CA009206.

[a]Also at Department of Radiology, University of Wisconsin-Madison, Madison, Wisconsin 53705; Electronic mail: gchen7@wisc.edu

[1]T. Weitkamp, A. Diaz, C. David, F. Pfeiffer, M. Stampanoni, P. Cloetens, and E. Zeigler, "X-ray phase imaging with a grating interferometer," Opt. Express **13**, 6296–6304 (2005).
[2]F. Pfeiffer, C. Grünzweig, O. Bunk, G. Frei, E. Lehmann, and C. David, "Neutron phase imaging and tomography," Phys. Rev. Lett. **96**, 215505 (2006).
[3]F. Pfeiffer, M. Bech, O. Bunk, P. Kraft, E. F. Eikenberry, C. Brönnimann,

C. Grünzweig, and C. David, "Hard-x-ray dark-field imaging using a grating interferometer," Nature Mater. **7**, 134–137 (2008).
[4]F. Pfeiffer, C. Kottler, O. Bunk, and C. David, "Hard x-ray phase tomography with low-brilliance sources," Phys. Rev. Lett. **98**, 108105 (2007).
[5]Z. Huang, K. Kang, L. Zhang, Z. Chen, F. Ding, Z. Wang, and Q. Fang, "Alternative method for differential phase-contrast imaging with weakly coherent hard x rays," Phys. Rev. A **79**, 013815 (2009).
[6]A. Momose, W. Yashiro, H. Kuwabara, and K. Kawabata, "Grating-based x-ray phase imaging using multiline x-ray source," Jpn. J. Appl. Phys. **48**, 076512 (2009).
[7]Z. Qi, J. Zambelli, N. Bevins, and G.-H. Chen, "Quantitative imaging of electron density and effective atomic number using phase contrast CT," Phys. Med. Biol. **55**, 2669–2677 (2010).
[8]J. Zambelli, N. Bevins, Z. Qi, and G.-H. Chen, "Radiation dose efficiency comparison between differential phase contrast ct and conventional absorption CT," Med. Phys. **37**, 2473–2479 (2010).
[9]J. Herzen, T. Donath, F. Pfeiffer, O. Bunk, C. Padeste, F. Beckmann, A. Schreyer, and C. David, "Quantitative phase-contrast tomography of a liquid phantom using a conventional x-ray tube source," Opt. Express **17**, 10010–10018 (2009).
[10]W. Yashiro, Y. Takeda, and A. Momose, "Efficiency of capturing a phase image using cone-beam x-ray Talbot interferometry," J. Opt. Soc. Am. A **25**, 2025–2039 (2008).
[11]A. Macovski, *Medical Imaging Systems* (Prentice-Hall, Englewood Cliffs, 1983).
[12]W. A. Kalender, *Computed Tomography: Fundamentals, System Technology, Image Quality, Applications* (Publicis, Erlangen, 2005).
[13]A. C. Kak and M. Slaney, *Principles of Computerized Tomographic Imaging* (IEEE, New York, 1988).
[14]T. J. Suleski, "Generation of Lohmann images from binary-phase Talbot array illuminators," Appl. Opt. **36**, 4686–4691 (1997).
[15]V. Arrizón and E. Lopez-Olazagasti, "Binary phase grating for array generation at 1/16 of Talbot distance," J. Opt. Soc. Am. A **12**, 801–804 (1995).
[16]O. Kafri and I. Glatt, *The Physics of Moir'e Metrology* (Wiley-Interscience, New York, 1990).
[17]A. Momose, S. Kawamoto, I. Koyama, Y. Hamaishi, H. Takai, and Y. Suzuki, "Demonstration of x-ray Talbot interferometry," Jpn. J. Appl. Phys., Part 2 **42**, L866–L868 (2003).
[18]G. Faris and R. Byer, "Three-dimensional beam-deflection optical tomography of a supersonic jet," Appl. Opt. **27**, 5202–5212 (1988).
[19]Z. Qi and G.-H. Chen, "Direct fan-beam reconstruction algorithm via filtered backprojection for differential phase-contrast computed tomography," X-Ray Optics and Instrumentation **2008**, 835172 (2008).
[20]Note that we have ignored the small-angle scattering contribution here. If small-angle scattering is included, the visibility of the fringe pattern will be reduced.
[21]Z. Huang, K. Kang, Z. Li, P. Zhu, Q. Yuan, W. Huang, J. Wang, and A. Yu, "Direct computed tomographic reconstruction for directional-derivative projections of computed tomography of diffraction enhanced imaging," Appl. Phys. Lett. **89**, 041124 (2006).
[22]C. David, J. Bruder, T. Rohbeck, C. Grünzweig, C. Kottler, A. Diaz, O. Bunk, and F. Pfeiffer, "Fabrication of diffraction gratings for hard x-ray phase contrast imaging," Microelectron. Eng. **84**, 1172–1177 (2007).
[23]E. Nickoloff and R. Riley, "A simplified approach for modulation transfer function determinations in computed tomography," Med. Phys. **12**, 437–437 (1985).
[24]F. Pfeiffer, T. Weitkamp, O. Bunk, and C. David, "Phase retrieval and differential phase-contrast imaging with low-brilliance x-ray sources," Nat. Phys. **2**, 258–261 (2006).